13th International Symposium on Particle Image Velocimetry – ISPIV 2019
Munich, Germany, July 22-24, 2019

Mach number influence on large-scale structures in ZPG turbulent boundary layers

Matthew Bross[1*], Sven Scharnowski[1], Christian J. Kähler[1]

[1] Universität der Bundeswehr München, Institute of Fluid Mechanics and Aerodynamics, Neubiberg, Germany

[*] matthew.bross@unibw.de

Abstract

Large-scale coherent structures in turbulent boundary layers (TBLs) have been of great interest in recent years. These meandering high- and low-momentum superstructures can extend up to several boundary layer thicknesses and contain a relatively large potion of the layer's turbulent kinetic energy. The characterization of these structures is important for understanding the overall dynamics of turbulent boundary layers and for the development of flow control strategies or near-wall flow modifications. However, compared to the extensive number of incompressible investigations much less is known about the structural characteristics for compressible turbulent boundary layer flows. Therefore, in this investigation turbulent boundary layers developing on a flat plate over a range of Reynolds numbers and Mach numbers are considered in order to investigate the effect of compressibility on coherent structures. More specifically, measurements are performed on a flat plate model in the Trisonic Wind Tunnel Munich (TWM) for $0.3 < \mathrm{Ma} < 3.0$ and a friction Reynolds number of $2700 < \mathrm{Re}_\tau < 14\,800$ or $19\,800 < \mathrm{Re}_{\delta_2} = \rho_e u_e \theta / \mu_w < 40\,800$. Velocity fields are recorded using planar particle image velocimetry methods (PIV and stereo-PIV) in three perpendicular planes, i.e. streamwise-wall-normal (xz), spanwise-wall-normal (yz), and wall-parallel (xy). Using multi-point statistical methods it was found that the streamwise spatial extent of coherent structures in the log-law layer slightly increases with increasing Mach number. Furthermore, a distinct increase in the spanwise spacing of these structures was found for the supersonic cases when compared to the subsonic and transonic turbulent boundary layers.

1 Introduction

The coherent structures present various wall boundary flows including zero pressure gradient (ZPG) turbulent boundary layers has been studied extensively in the past decades and many statistical and structural properties of the flow are well known, as documented in the extensive review by Wallace (2012). High- and low-momentum large-scale coherent motions residing in the log-law layer called superstructures have been of particular focus in the last two decades, Adrian et al. (2000); Ganapathisubramani et al. (2005); Hutchins and Marusic (2007); Monty et al. (2009); Buchmann et al. (2016). A fascinating property of the superstructures is their streamwise length which is on average about $6\delta - 8\delta$. However, instantaneously they can extend up to $10\delta - 20\delta$ in the streamwise direction, making their characterization in both experiments and simulations challenging due to the large field of view required. These structures also strongly meander in the spanwise direction (Hutchins et al., 2011) and it has been shown that they can carry a relatively large a portion of the layer's turbulent kinetic energy, especially at large Reynolds numbers. In effect, these large-scale structures are the main contribution to the formation of the plateau/peak in the streamwise velocity fluctuations in the log-law layer, which appears at high Reynolds numbers (Fernholz and Finley, 1996; Monty et al., 2009; Samie et al., 2018). Therefore, the investigation of these superstructures is important for understanding the overall dynamics of turbulent boundary layers. However, compressibility effects on the coherent structures is by far less studied, mostly due to the many technical challenges these types of flow present.

One of the first direct comparisons of compressible and incompressible turbulent boundary layers was done by Smits et al. (1989) using the correlated signals from a traversed hotwire for $\mathrm{M} = 0.1$ and 2.9. They concluded that the spanwise spacing of correlated streamwise features remains unchanged for the

subsonic and supersonic cases, but the streamwise length of the correlated mass flux fluctuations $(\rho u)'$ regions were twice as big for the subsonic case when compared to the supersonic case. Furthermore, a survey done by Smits and Dussauge (2006) of available supersonic measurements, mostly using hot-wire probes, concluded that for increasing Mach number and Reynolds number the streamwise length scales decrease significantly while the spanwise scales remain unaffected by both Reynolds number and Mach number.

In addition to point-wise probe measurements such at hot-wire anemometry, particle image velocimetry (PIV) has been used as a tool both visualize and analyze the structural properties of supersonic boundary layers. In the work of Ganapathisubramani et al. (2006), elongated streamwise coherent structures in a turbulent boundary layer at Mach 2 at Re_θ = 35 000 (Re_τ = 5600) were visualized by using planar PIV in streamwise-spanwise planes (wall parallel), where an underlying similarity to incompressible superstructures was observed. However, two-point correlations of velocity fluctuations revealed that the streamwise lengths scales for a Mach 2 turbulent boundary layer were as much as 4 times larger than an incompressible case while the spanwise spacing remains similar to the incompressible case. The increase in streamwise length scales with Mach number is in contrast to the survey of hot-wire measurements provided in Smits and Dussauge (2006), however they attribute this to a Reynolds number effect or the difference between $(\rho u)'$ and u' correlations. Furthermore, direct numerical simulations of a Ma = 2 turbulent boundary layer at Re_τ = 1120 or Re_{δ_2} = 3900 show that the streamwise velocity length scales do not change when compared to the incompressible case, while the spanwise wavelengths are slightly larger for the computed supersonic flow when compared to experimental incompressible data, Pirozzoli and Bernardini (2011).

Large-scale coherent motions were also identified in a Mach 3 turbulent boundary layer in a direct numerical simulation up to $\mathrm{Re}_\theta < 2600$ by Ringuette et al. (2008). The alternating high and low-speed structures were identified in the log-law layer with a average spanwise width of 0.4δ based on $(\rho u)'$ and u' correlations. They also looked at the extent of low-speed structures at a wall-normal location of $z/\delta = 0.2$ by extending simulated time domain to spacial distance with Taylor's Frozen turbulence hypothesis and found in contours of instantaneous u-velocity, low-speed structures up to 100δ in length. These results were then compared to the incompressible turbulent boundary layer hot-wire measurements of Hutchins and Marusic (2007) and found the the superstructures for both incompressible and compressible were similar, despite the order of magnitude difference in Reynolds number. While the extent of instantaneous structures could not be truly compared because of the effective spatial domain of the hot-wire measurements was around 20δ, Ringuette et al. (2008) state that the spanwise spaing of the structures for both cases is about 0.5δ. In comparison, Elsinga et al. (2010) used tomographic-PIV to investigate structures in a turbulent boundary layer at Mach 2 and much larger Reynolds number than in Ringuette et al. (2008), Re_θ = 34 000. They identified three-dimensional packages of elongated structures in the log-layer where the typical width of low-speed regions varied between 0.25δ and 0.4δ and spanwise spacing between 0.5δ to 1δ.

As the past experiments performed in different facilities do not lead to consistent results. The motivation for the current study is to investigate experimentally the structural topology of large scale structures at subsonic, transonic, and supersonic Mach numbers in the same test facility by means of state-of-art PIV techniques. The analysis consider the characteristic streamwise and spanwise scales of superstructures in the log-law layer over a Mach number range $0.3 < \mathrm{Ma} < 3.0$.

2 Experimental Facility

The Trisonic Wind Tunnel Munich (TWM) is a blow-down type wind tunnel with a 300 mm $\times$ 675 mm (width $\times$ height) test section. A two-throat system consisting of an adjustable Laval nozzle and an adjustable diffuser allows for a stable operating Mach number range from 0.2 to 3.0. The stagnation pressure is controlled by a pressure regulation valve and is adjustable between $p_0 = 1.2\,\mathrm{bar}$ and $5.0\,\mathrm{bar}$. This allows to set the Reynolds number independently of the Mach number. The corresponding Reynolds number range is $(4-78)\times 10^6\,\mathrm{m}^{-1}$. The stagnation pressure p_0 and temperature T_0 are recorded by two sensors in the settling chamber. The facility has two holding tanks that can be pressurized up to 20 bar above ambient pressure, with each tank holding a volume of 178 m^3 of air. This amount of air is sufficient for run times in the order of 100 seconds for the cases discussed below. The wind tunnel's test section is enclosed by a plenum chamber and also has the ability to apply boundary layer suction at both the vertical and the horizontal walls independently. A more detailed description of the freestream velocity and pressure fluctuations in the TWM can be found in Scharnowski et al. (2018).

Table 1: Flow field properties.

Ma_e		0.3	0.8	2.0	3.0
p_0	[bar]	1.5	1.5	2.2	4.5
t_0	[K]	288	288	287	288
t_e	[K]	282	255	160	103
ρ_e	[kg/m^3]	1.74	1.34	0.614	0.415
μ_e	[N s/m^2]$\times 10^{-5}$	1.76	1.63	1.09	0.71
ν_e	[N^2/s]$\times 10^{-5}$	1.02	1.21	1.77	1.75
u_e	[m/s]	101	256	506	610
t_w	[K]	289	288	283	283
ρ_w	[kg/m^3]	1.70	1.19	0.346	0.150
μ_w	[N s/m^2]$\times 10^{-5}$	1.79	1.79	1.77	1.77
ν_w	[N^2/s]$\times 10^{-5}$	1.06	1.50	5.01	11.7

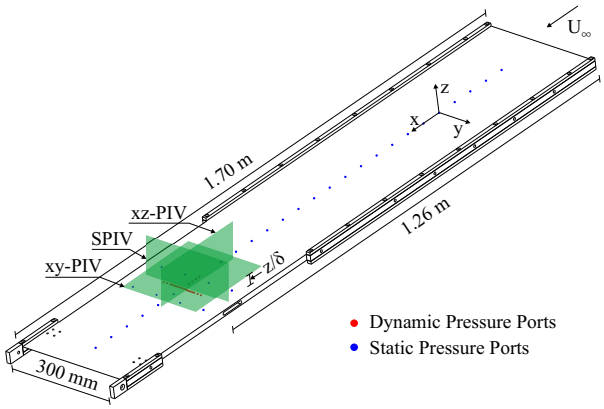

Figure 1: Flat plate boundary layer model used in Trisonic Wind Tunnel Munich (TWM). Planar PIV measurement planes location and orientation are indicated and labeled. Flow direction coordinates (x, y, z) correspond to streamwise, spanwise and wall-normal directions respectively.

A flat plate boundary layer model was mounted in the test section of the TWM for this investigation. A sketch of the model and coordinate system is shown in figure 1. The overall length of the model in the streamwise direction is 1.70 m, resulting in a turbulent boundary layer thickness of $13 - 20$ mm at the measurement location, 1.26 m downstream of the leading-edge. Furthermore, a resistance based temperature sensor was installed just under the top surface, via a milled out cavity on the bottom side, in order to estimate the wall temperature T_w.

The freestream fluid properties in the settling chamber and the test section are outlined in table 1. The fluid properties in the freestream are calculated using the isentropic expansion equations and are denoted with the subscript e, e.g. the edge temperature T_e. Since the temperature of wall is known and the static pressure at the edge is the same at the wall ($p_e = p_w$), ρ_w can be calculated from the ideal gas law. The viscosity at the wall and the edge is estimated from the Sutherland Modell (Smits and Dussauge, 2006).

3 Mean Velocity Field

The mean streamwise velocity profile shown in figure 2(a) was calculated by transforming the u velocity component with the van-Driest transformation (Van Driest, 1951), see equations (1) and (2). This transformation takes into account the temperature at the wall and the edge. For sub-hypersonic Mach numbers the transformation is sufficiently valid (Smits and Dussauge, 2006). Then the transformed velocity is fit to the standard logarithmic "Law-of the Wall" plus the Coles correction factor, see equation (3). The mean flow parameters are outlined in table 2. What is important to note is the Reynolds number, namely the classical incompressible wall-turbulent Reynolds number Re_τ becomes small for Ma = 2.0 and 3.0 despite having

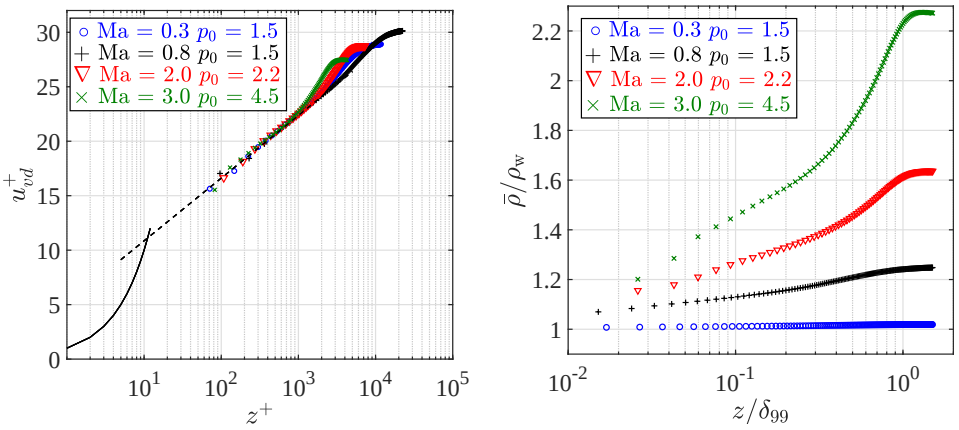

(a) (b)

Figure 2: (a) Inner scaled Van-Driest transformed u_{vd}^+ mean velocity profile for $0.3 < \mathrm{Ma} < 3.0$. (b) Mean density $\bar{\rho}$ normalized with fluid density at the wall ρ_w profile in the wall normal (z) direction.

Table 2: Boundary layer parameters.

Ma_e		0.3	0.8	2.0	3.0
δ_{99}	[mm]	24.5	26.9	14.0	14.1
Π	[-]	0.28	0.19	0.47	0.55
u_τ	[m/s]	3.41	8.42	18.3	23.8
Re_τ	[-]	7785	14 888	4807	2790
Re_θ	[-]	19 679	43 684	41 564	60 297
Re_{δ_2}	[-]	19 886	40 803	26 275	24 916

large u_τ. This is because the kinematic viscosity at the wall is large and therefore a more useful Reynolds number to compare incompressible and compressible is $\mathrm{Re}_{\delta_2} = \rho_e u_e \theta / \mu_w$. The edge flow properties are calculated by assuming an isentropic expansion by the Laval nozzle. Since the static pressure at the edge is the same at the wall according to boundary layer theory and the wall temperature T_w is measured, the density at the wall can be calculated from the ideal gas law. The kinematic viscosity at the wall can then be calculated via the Sutherland-Modell (Smits and Dussauge, 2006).

$$u^* = \frac{u_e}{b} \sin^{-1}\left(\frac{2b^2(u/u_e) - a}{\sqrt{a^2 + 4b^2}}\right) \tag{1}$$

$$a = \left(1 + r\frac{\gamma - 1}{2} Ma_e^2\right)\frac{T_e}{T_w} - 1; b = r\frac{\gamma - 1}{2} Ma_e^2 \frac{T_e}{T_w} \tag{2}$$

$$u_{vd}^+ = \frac{u^*}{u_\tau} = \frac{1}{\kappa}\log\left(\frac{u_\tau z}{\nu_w}\right) + C^* + \frac{2\Pi}{\kappa}\sin^2\left(\frac{\pi}{2}\frac{z}{\delta_c}\right) \tag{3}$$

4 Structural Analysis

To give an overview of the turbulent boundary layer characteristics the streamwise development of the turbulent boundary layer in the streamwise-wall-normal (xz-plane) is considered in this section, see figures 3(a) and 3(b) for an exemplary instantaneous velocity field at Ma = 0.3 and Ma = 2.0. The long streamwise extent of the measurement plane is achieved by stitching together two overlapping fields of view from a side-by-side camera arrangement.

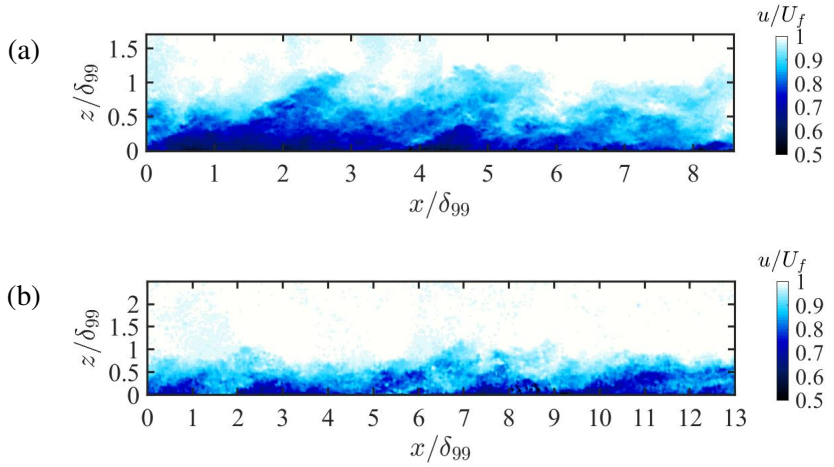

Figure 3: Instantaneous velocity field u/U_f in the xz-plane where $U_f = 0.99U_\infty$ at (a) Ma = 0.3 and p_0 = 1.5 and (b) Ma = 2.0 and p_0 = 2.2.

To confirm this, the spatial spectral density was calculated for Ma = 0.3 and 2.0 and is plotted in figures 4(a) and 4(a). In these plots the highest value contour level of the normalized pre-multiplied velocity spectra, $(\bar{\rho}/\rho_w)k_x\Phi_{uu}/u_\tau^2$, appears at a streamwise wave length of $\lambda_x/\delta_{99} \approx 2.5$ and 3.5 for Mach 0.3 and 2.0 respectively. While measurements closer to the wall were not possible in these experiments, this peak in the spatial spectral plots is related to the secondary peak (Fernholz and Finley, 1996; Monty et al., 2009; Samie et al., 2018) in the streamwise velocity fluctuations. Since this peak is associated with the meandering superstructures in the log-law layer, it can be concluded that the superstructures are slightly more energetic for Ma = 2.0 as compared to 0.3 in the measurements presented herein even though the friction based Reynolds number is larger for Ma = 0.3 (Re_τ = 7785) than Ma = 2.0 (Re_τ = 4807), demonstrating that Re_τ is not a good reference value for comparing compressible and incompressible boundary layers.

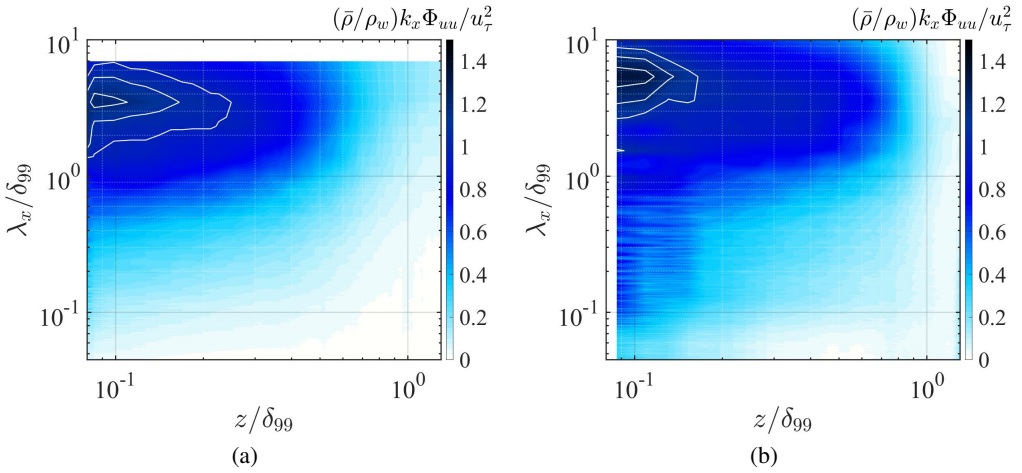

Figure 4: Streamwise (u) pre-multiplied spectral density map, where wall distance z and streamwise energy wave length λ_x are both scaled with δ_{99} for (a) Ma = 0.3 and (b) Ma = 2.0 cases. Solid white contour lines correspond to contour levels $(\bar{\rho}/\rho_w)k_x\Phi_{uu}/u_\tau^2$ = 1.1, 1.2 and 1.3.

In order to visualize and analyze the organization of coherent flow structure in the spanwise direction at different wall normal heights, a stereo PIV measurement was performed in a cross-stream plane for all Mach numbers. The characteristic spatial distribution of coherent features in the spanwise direction via multi-point statistics and spatial spectral calculations are presented in the following.

To compare the spanwise spacing of coherent structures as a function of Mach number, slices of the correlation R_{uu} and R_{uw} at $z/\delta_{99} = 0.2$ for Ma = 0.3, 0.8, 2.0, and 3.0 are plotted in figures 5(a) and 5(b). In this figure, the spanwise (y-direction) shift is represented as ξ_y, where $\xi_y = y_o + \Delta y$ and y_0 is the center of the field of view in the spanwise direction. For all Mach numbers, there is a central positive correlation peak flanked on either side by a smaller negative correlation. However, the spacing between the negative correlation peaks is distinctly different for Ma = 0.3 and 0.8 when compared to the supersonic cases at Ma = 2.0 and 3.0. For the subsonic cases the spacing between the negative correlations is $0.8\delta_{99}$ compared to the a spacing closer to $1.2\delta_{99}$ for the supersonic cases.

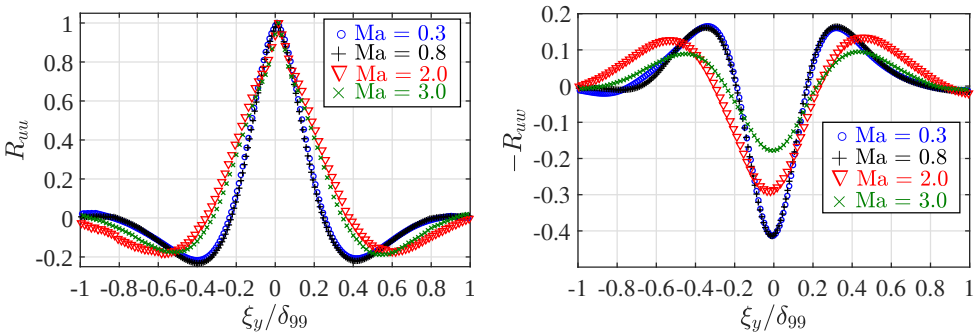

Figure 5: Spanwise distribution of (a) R_{uu} and (b) R_{uw} for Ma = 0.3, 0.8, 2.0, and 3.0 at $z/\delta_{99} = 0.2$. On the horizontal axis $\xi_y = y_0 + \Delta y$ where y_0 is the center of the field of view in the spanwise direction.

This finding is confirmed at different wall normal distances in the spectrogram plot shown in figures 6(a) and 6(b). In this plot the spectra of the streamwise velocity pre-multiplied with the spanwise wave number as a function of spanwise wave lengths and wall normal distance for Ma = 0.3 and Ma = 2.0 are shown. According to these plots the most energetic spanwise wavelengths for the subsonic case are less than λ_y/δ_{99} and generally remain below that value for increasing wall normal distance. Contrary to this, the most energetic wavelengths in the log-law region of the supersonic case are slightly above λ_y/δ_{99}, which is consistent with the findings in figure 5(a). This demonstrates, that the effect of Mach number is to increase the spanwise spacing of the coherent structures.

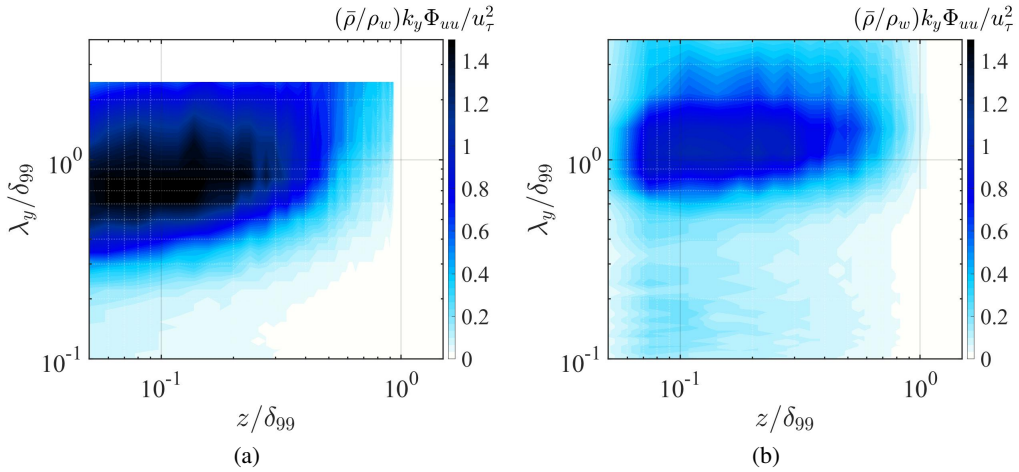

Figure 6: Pre-multiplied spanwise spectral density for (a) Ma = 0.3 and (b) Ma = 2.0 cases.

To confirm that long high- and low-momentum meandering superstructures exist in the log-law region over the range of Mach numbers investigated, PIV measurements in a wall-parallel plane (xy) were performed. An exemplary instantaneous field in this plane is provided in figure 7(a) for Ma = 3.0. What is

immediately evident in these figures is the meandering streaky structures, confirming the existence of superstructures in supersonic flows. Clearly, the large scale structures or superstructures are present in have a streamwise extent of several δ_{99} and a spanwise spacing of around $1\delta_{99}$.

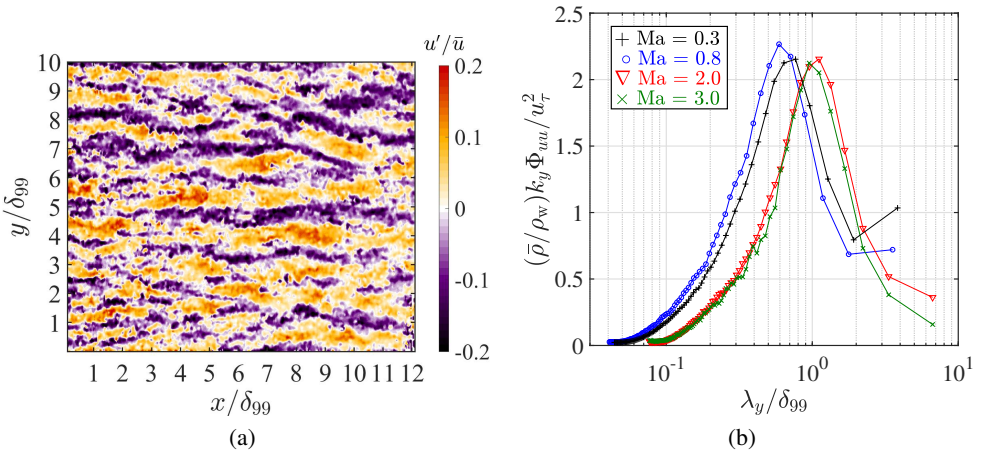

Figure 7: (a) Instantaneous streamwise velocity fluctuation fields in the *xy* plane for Ma = 3.0. Measurement plane location at $z/\delta_{99} = 0.2$. (b) Pre-multiplied spanwise direction spectral density slices for $0.3 < \text{Ma} < 3.0$.

To further investigate the spacing in the spanwise direction and confirm the result from the previous figures where it was demonstrated that the spanwise spacing of structures was larger for the supersonic case in comparison to the subsonic case, the spectral density of the streamwise velocity fluctuations in the spanwise direction was calculated and plotted in 7(b). In this plot the location of the peak in the energy spectra is location just below $\lambda_y/\delta_{99} = 1$ for both subsonic cases and slightly larger than $\lambda_y/\delta_{99} = 1$ for the supersonic cases. While the location of the wall-parallel measurement plane was at slightly different z/δ_{99} for the subsonic and supersonic cases due to the changing boundary layer thickness, the finding that the structure spacing is larger for supersonic as compared to subsonic is consistent with the finding in the previous section.

5 Concluding Remarks

In this work, turbulent boundary layers developing on a flat plate over a range of $0.3 < \text{Ma} < 3.0$. are measured with planar 2D and stereo-PIV. It is important to note that the comparison of subsonic, transonic, and supersonic turbulent boundary layers is done in the same wind tunnel facility, were the flow quality is well documented for the range of Mach numbers considered, Scharnowski et al. (2018).

It was demonstrated in this work that the van Driest scaling of the mean velocity profile produced a good collapse of profiles over the range of Mach numbers investigated. Furthermore, it was shown that the friction based Reynolds number, which is commonly used to characterize incompressible wall bounded turbulence, is not as useful for compressible turbulence due to the large viscosity found near the wall which leads to relatively small friction based Reynolds numbers despite extremely large u_τ.

Furthermore, multi-point statistical and spatial spectral methods were used to determine the spacing and spatial extent of large scale features in the streamwise and spanwise directions. It was shown that large-scale coherent motions exist in supersonic boundary layers qualitatively similar to the incompressible cases found in literature. Which is in contrast to decrease in streamwise mass flux correlation with increasing Mach number shown in Smith and Smits (1995).

Finally, a distinct increase in the spanwise spacing of large-scale structures in the supersonic cases as compared to the Ma = 0.3 and 0.8 cases was demonstrated. In addition, it was also noticed that the spanwise spacing slightly increased with increasing Mach number, albeit only around 15%, in the DNS results of Pirozzoli and Bernardini (2011). However, experimental investigations, either hotwire or PIV, have not reported a variation in the spanwise spacing with Mach number.

Acknowledgements

This work is supported by the Priority Programme SPP 1881 Turbulent Superstructures funded by the Deutsche Forschungsgemeinschaft project number KA1808/21-1.

References

Adrian RJ, Meinhart CD, and Tomkins CD (2000) Vortex organization in the outer region of the turbulent boundary layer. *J Fluid Mech* 422:1–54

Buchmann NA, Kücükosman YC, Ehrenfried K, and Kähler CJ (2016) Wall pressure signature in compressible turbulent boundary layers. in *Progress in Wall Turbulence 2*. pages 93–102. Springer International Publishing

Elsinga GE, Adrian RJ, van Oudheusden BW, and Scarano F (2010) Three-dimensional vortex organization in a high-reynolds-number supersonic turbulent boundary layer. *J Fluid Mech* 644:35–60

Fernholz HH and Finley PJ (1996) The incompressible zero-pressure-gradient turbulent boundary layer: An assessment of the data. *Progress in Aerospace Sciences* 32:245–311

Ganapathisubramani B, Clemens NT, and Dolling DS (2006) Large-scale motions in a supersonic turbulent boundary layer. *J Fluid Mech* 556:271–282

Ganapathisubramani B, Hutchins N, Hambleton WT, Longmire EK, and Marusic I (2005) Investigation of large-scale coherence in a turbulent boundary layer using two-point correlations. *J Fluid Mech* 524:57–80

Hutchins N and Marusic I (2007) Evidence of very long meandering features in the logarithmic region of turbulent boundary layers. *J Fluid Mech* 579:1–29

Hutchins N, Monty JP, Ganapathisubramani B, NG HCH, and Marusic I (2011) Three-dimensional conditional structure of a high-reynolds-number turbulent boundary layer. *J Fluid Mech* 673:255–285

Monty JP, Hutchins N, NG HCH, Marusic I, and Chong MS (2009) A comparison of turbulent pipe, channel and boundary layer flows. *J Fluid Mech* 632:431–442

Pirozzoli S and Bernardini M (2011) Turbulence in supersonic boundary layers at moderate reynolds number. *J Fluid Mechanics* 688:120168

Ringuette MJ, Wu M, and Martín MP (2008) Coherent structures in direct numerical simulation of turbulent boundary layers at mach 3. *J Fluid Mech* 594:59–69

Samie M, Marusic I, Hutchins N, Fu MK, Fan Y, Hultmark M, and Smits AJ (2018) Fully resolved measurements of turbulent boundary layer flows up to $Re_\tau = 20000$. *J Fluid Mech* 851:391–415

Scharnowski S, Bross M, and Kähler CJ (2018) Accurate turbulence level estimations using piv/ptv. *Exp Fluids* 60:1

Smith MW and Smits AJ (1995) Visualization of the structure of supersonic turbulent boundary layers. *Exp Fluids* 18:288–302

Smits AJ and Dussauge JP (2006) *Turbulent Shear Layers in Supersonic Flow*. Springer

Smits AJ, Spina EF, Alving AE, Smith RW, Fernando EM, and Donovan JF (1989) A comparison of the turbulence structure of subsonic and supersonic boundary layers. *Phy of Fluids A* 1:1865–1875

Van Driest ER (1951) Turbulent boundary layer in compressible fluids. *J Aero Sci* 18:145–160

Wallace JM (2012) Highlights from 50 years of turbulent boundary layer research. *J Turbulence* 13:1–70